Available online at www.sciencedirect.com
ScienceDirect
Journal of Bionic Engineering 12 (2015) 406–417

Bio-inspired Flow Sensing and Prediction for Fish-like Undulating Locomotion: A CFD-aided Approach

Han Zhou[1], Tianjiang Hu[1,2], Kin Huat Low[3], Lincheng Shen[1] , Zhaowei Ma[1], Guangming Wang[1], Haijun Xu[1]

1. *College of Mechatronics and Automation*, *National University of Defense Technology*, *Changsha* 410073, *China*
2. *State Key Laboratory of High Performance Computing*, *National University of Defense Technology*, *Changsha* 410073, *China*
3. *School of Mechanical and Aerospace Engineering*, *Nanyang Technological University, Singapore* 639798

Abstract

Feedback flow information is of significance to enable underwater locomotion controllers with higher adaptability and efficiency within varying environments. Inspired from fish sensing their external flow via near-body pressure, a computational scheme is proposed and developed in this paper. In conjunction with the scheme, Computational Fluid Dynamics (CFD) is employed to study the bio-inspired fish swimming hydrodynamics. The spatial distribution and temporal variation of the near-body pressure of fish are studied over the whole computational domain. Furthermore, a filtering algorithm is designed and implemented to fuse near-body pressure of one or multiple points for the estimation on the external flow. The simulation results demonstrate that the proposed computational scheme and its corresponding algorithm are both effective to predict the inlet flow velocity by using near-body pressure at distributed spatial points.

Keywords: bio-inspired fish undulating locomotion, flow sensing, near-body pressure, flow velocity estimation, Computational Fluid Dynamics (CFD)

doi: 10.1016/S1672-6529(14)60132-3

1 Introduction

Fish are capable to adapt natural selection by developing distinctive and remarkable ability of movement in the water in order for prey, escaping from predators, reproduction and cluster migration. Fish possess a good environmental adaptability in addition to their streamline shape profile and skin micro-structure, fluctuations or oscillating propulsion mode[1–3]. Fish can sense the slow transformation of surrounded flow fields by biological sensing organs, so as to keep sustained speed under lower energy consumption and higher efficiency[1,3–5]. They can also achieve high mobility under explosion speed. Lateral line plays an important role as the key component of fish perception system. It enables fish to detect wide-scale, ambient water motion created by wind and gravity, and local water disturbance created by animal movements or by the interaction between ambient water motion and aquascape features. Lateral line system includes Superficial Neuromast (SN) subsystem and Canal Neuromast (CN) subsystem. SNs lie in fish body surface and CNs are buried deep in lateral line canal. Research found that SNs perceive external fluid velocity, while CNs perceive external fluid acceleration associated with external fluid pressure[6]. Despite the diversity of trunk canal patterns, one trunk canal typically extends along the fish body to the caudal peduncle (Fig. 1)[7].

Most of the robotic fish were developed to demonstrate bionic wave propulsion, but the robotic fish did not perform as well as real fish in terms of swimming capability. The improvement of the performance is still an ongoing work[8–15]. A series of studies have shown the ability of pressure sensing on imitating the function of lateral line systems[16–28], though real fish do not have neuromasts that directly measure pressure. Pressure sensing applications reported in the literature include dipole source localization[17,18], object recognition[19,20], flow pattern detection such as steady uniform flow and unsteady periodic flow[21,22]. The artificial lateral line system would be beneficial for the performance improvement of underwater vehicle. The ability to obtain

Corresponding author: Tianjiang Hu
E-mail: t.j.hu@nudt.edu.cn

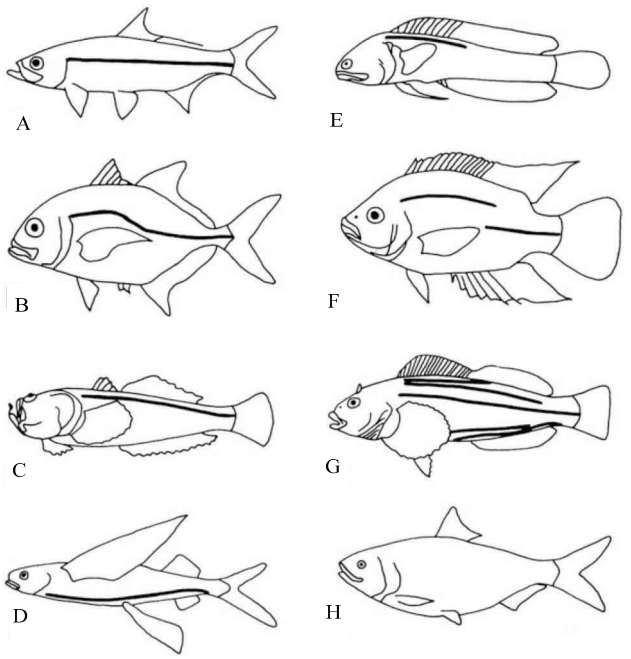

Fig. 1 Lateral line along with fish body among teleost fishes. Many fish species have one or more lateral lines. One trunk canal typically extends down the length of the body to the caudal peduncle. (A) Complete straight; (B) complete arched; (C) dorsally placed; (D) ventrally placed; (E) incomplete; (F) disjunct; (G) multiple and (H) absent. (Adapted from Ref. [7]).

information about obstacles enables a prospective application for complex underwater environment observation, and the ability of flow mapping allows the possibility for optimizing energy efficiency and improving the performance of motion control. Distributed pressure measurements are used to estimate the orientation of streamline body and the free-stream flow speed, and to enhance a feedback controller[23,24]. Salumäe and Kruusmaa apply pressure sensing to achieve flow-relative and flow-aided navigation, such as speed control, orientation and station holding in the Kármán street[25]. Ježov *et al*. reduce robotic fish energy consumption in turbulence by exploiting vorticity based on pressure measurements[26]. Most artificial line systems are demonstrated on a rigid body, such as plane, airfoil or rigid body of fish. However, undulation and periodicity are typical characteristics in biomimetic fish-like swimming, thus hydrodynamic physical quantities present undulation and periodicity, such as near-body pressure. Previous works[23–28] are important to progressively characterize the hydrodynamic signatures by pressure sensing. However, to better understand the effects of pressure signals, the study on the temporal-and-spatial profiles and their effects by self-motion will be useful. Lateral-line inputs will provide information about the body motion and the resulting activity in the sensing organ[27]. Akanyeti *et al*. used onboard pressure sensors to measure the pressure profiles while moving forward and backward harmonically, and presented the relationship between the craft motion and pressure signals across varying swimming speeds[28]. Nevertheless, self-generated signals caused by wave motion should be further considered besides those related to moving speed.

Experiments of real fish have seldom repeatedly been carried into execution easily, due to the unpredictable response of live fish and the non-repeatability of measurements. An alternate approach is to use model-based computational methods. The computational methods, *e.g*. Computational Fluid Dynamics (CFD) for fish-like locomotion, are definitely repetitive for various scenarios and sufficiently characterize multiple phenomena such as viscous effects, boundary layer separation and vortex shedding. The CFD method solves and analyses problems involving a fluid flow by numerical simulations. The simulations generate numerical data describing the hydrodynamic characteristics of the whole computational domain. Liu *et al*. proposed a time-accurate solution of Navier-Stokes equations to solve unsteady hydrodynamics around an undulatory swimming body[29]. Since then, CFD models have been extensively exploited to understand the specific mechanism of underwater bionic swimming[30–34]. Some robotic fish experiments shows good agreement with the CFD results[35]. On the other hand, CFD is also used to calculate the stimulus to the lateral line of a fish[36–38] and the unsteady flow inside the lateral line trunk canal of the fish[39]. Inspiringly, it is validated that pressure sensing values matched approximately between those by respective CFD simulations and experiments[24,37–38].

This paper employs a CFD-aided approach to understand bio-inspired flow sensing and prediction via distributed near-body pressure. Pressure sensing on specified near-body points satisfies the requirements of practical applications, although the whole domain pressure information is available within the computational scheme. Firstly, fish-like swimming hydrodynamics is numerically solved to provide pressure distribution within the whole computational domain. Secondly, several virtual pressure sensors inspired by lat-

eral line are designed to collect pressure data on fish body surface. Thirdly, distributed near-body pressure is fused into estimation on the surrounding flow. Finally, scenarios of time-varying flow inlets are conducted to validate the effectiveness of the proposed CFD-aided approach for bio-inspired flow sensing and prediction.

2 Computational flow sensing scheme

2.1 Near-body pressure versus flow patterns

The relationship between near-body pressure and flow pattern is concentrated in the computation-aided flow sensing scheme. Once near-body pressure at given points has been obtained, the flow pattern can then be estimated from the pressure. In this study, virtual pressure sensors are allocated on fish body surface. Near-body pressure data is captured during the numerical simulation of fish swimming.

Bionic fish-like swimming is a dynamical process of energy transformation back and forth between the pressure and the kinetic energy. Unsteady Bernoulli principle, describing the power conservation law under an ideal fluid assumption, is given by

$$z - p - \frac{\rho v^2}{2} = \frac{\partial \phi}{\partial t}, \tag{1}$$

where z is related to the constant gravitational potential, p is statistic pressure, $\rho v^2/2$ represents flow kinetic energy, and ϕ is velocity potential. In steady flow, the right term of Eq. (1) can be treated as a constant. As a result, the work on fluid by pressure is equal to the change of fluid kinetic energy. Pressure decreases while velocity v increases. In fish-like swimming, we consider that velocity potential depends on the flow initial condition and the active wave motion of fish body. Obviously, they both affect the near-body pressure.

Energy transforming process is analyzed by ignoring the friction heat caused by viscosity, as shown in Fig. 2. The total energy in flow field comes from two sources: initial flow power and the power from fish active deformation. Initial flow power mainly contains gravitational potential, pressure energy and kinetic energy. The energy in the influenced flow field during fish-like swimming includes flow power and the energy of moving fish body. Energy in flow field is characterized by both the velocity and pressure. During fish-like swimming, the fluid kinetic energy is transferred into pressure energy, and then is turned into fish kinetic energy, and vice versa. For example: flow with velocity stagnates when it is blocked at the head of fish body; meanwhile the flow kinetic energy is converted into pressure energy. As a result, the pressure on the head point increases.

2.2 Flow computational platform

Fish use lateral line to sense flow information and avoid underwater obstacles. Biological mystery has attracted great attention from scientists and engineers. It is interesting to understand why and how the lateral line can sense flow information. Under such circumstance, computational scheme is proposed and developed to further promote understanding the lateral line system. The computation-aided flow sensing scheme employs CFD to transfer fish-like kinematics into digital hydrodynamics.

CFD method is a computational hydrodynamics way to numerically solve Navier-Stokes equations and visualize flow field. The entire computational domain is defined by $\Omega = \Omega_f \cup \Omega_b$, where the domain Ω_f is filled with fluid of constant density ρ and dynamic viscosity μ. The boundary Ω_b denotes fish body surface. The computational domain Ω is discretized in space by employing an unstructured, triangular mesh during pre-processing. A simulation of fish swimming is basically to solve the following problems: any deformed body motion and initial flow condition are defined (*i.e.*, fish kinematics and flow pattern). Next, the incompressible Navier-Stokes equations are discretized and evaluated in the computational domain. Finally, the hydrodynamic forces on the body are numerically evaluated, as well as the resulting flow field, especially the near-body pressure concerned, as shown in Fig. 3.

2.3 Computational pressure sensing

A fish swims in a uniform flow field with inlet velocity, heading in the opposite direction of flow speed. Fish body deforms according to kinematics law. Its centroid position and orientation angle are both fixed through the simulations. Body wave travels in the same direction of inlet flow velocity. The computational domain is shown in Fig. 4. Fish active body deformation results in high and low pressure areas symmetrically and alternately distributed near the body. As the wave propagates along with fish body, the high and low

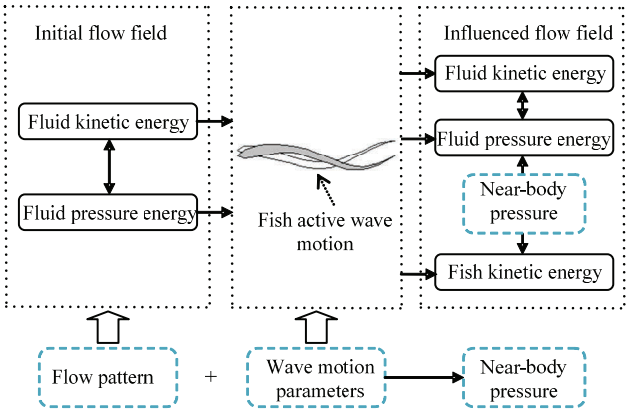

Fig. 2 Energy transforming process in fish-like swimming. Flow pattern defines the initial flow energy, and wave motion parameters describe fish active wave motion. They both have effects on near-body pressure.

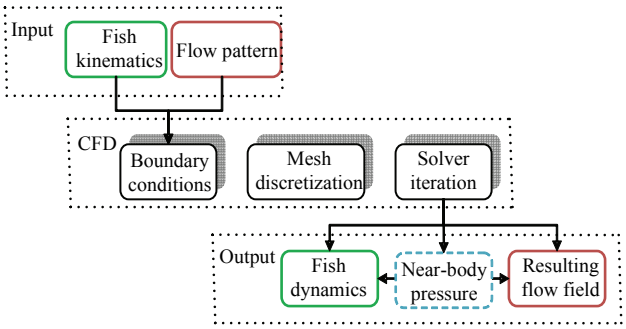

Fig. 3 CFD-aided flow sensing scheme in which fish kinematics and flow pattern are given as inputs. Hydrodynamics surrounding fish body are numerically calculated by CFD. Influenced flow field features are output after post-processing, especially near-body pressure concerned.

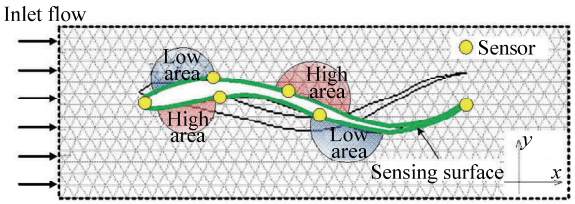

Fig. 4 Computational pressure sensing in uniform flow. High pressure areas and low pressure areas locate along with fish body alternately, and virtual pressure sensors are utilized to sensing near-body pressure.

pressure areas move backward from anterior body. The computational domain including fish body surface is discretized into mesh grid. Note that the minimum sampling interval of flow sensing is determined by the grid size. Considering the practical application in future, finite virtual pressure sensors are set on fish surface to collect near-body pressure, such as head end, body symmetry positions and adjacent positions, *etc*.

3 Flow information filtering and estimation algorithm

The relationship between statistical coefficients of near-body pressure and inlet flow velocity will be discussed. Pressure coefficients are obtained after the pressure data filtering. We will study how inlet flow velocity affects pressure coefficients, while fish swims with known wave motion parameters. The aim of the study is to estimate the inlet flow velocity by using pressure coefficients.

3.1 Pressure processing algorithm

The flow field is set as steady flow with inlet velocity U. The propulsive force mainly comes from pressure difference, and viscous force is small due to the high Reynolds number. Inlet velocity would affect surrounding flow of fish. These influences can be characterized by near-body pressure. On the other hand, wave motion causes the cyclic hydrodynamics of flow field around fish body. In general, factors affecting the pressure include time, sampling position, relative velocity and wave parameters. The present work considers pressure cyclical changes, pressure distribution along body surface, relationship between the pressure and flow velocity, and the relationship between pressure and wave motion parameters. Two questions will be presented: whether near-body pressure can reflect the flow inlet velocity? How to make use of near-body pressure to estimate flow inlet velocity? Pressure sensor information fusion can be further considered for the realization of flow velocity estimation, such as special difference, time average, variance, *etc*.

Under the CFD scenarios, the near-body sensors definitely obtain the distributed pressure data at the sampling times. It is necessary to define the stochastic parameters that have relationship with the flow velocity. In this study, these stochastic parameters are defined by the temporal-and-spatial operators, as follows

(1) Temporal average operator

$$\text{Average } \{p\}: \ \overline{p} = \frac{\int_{t-T_0}^{t} p \mathrm{d}\tau}{T_0}$$

(2) Temporal amplitude operator

Amplitude $\{p\}$:

$$Amp = \frac{\max\{p \,|\, \tau \in [t-T_0, t]\} - \min\{p \,|\, \tau \in [t-T_0, t]\}}{2}$$

(3) Temporal shift operator

Shift $\{p, \Delta t\}$: $p(t) = p(t - \Delta t)$

(4) Spatial sum operator

Sum $\{p_i\}$: $S = \sum_{i=1}^{n} p_i / n$, $\tau \in [t - T_0, t]$, n is the total number of sensors.

(5) Spatial difference operator

Differ $\{p_i, p_j\}$: $D = p_i - p_j$, $\tau \in [t - T_0, t]$, i and j represent the ith and jth sensors.

Pressure p obtained from the sensors can be expressed in dimensionless form. The normalization function is given by

$$C_p = \frac{p}{0.5\rho U^{*2}}.$$

where C_p is normalized pressure coefficient and $U^* = \lambda/T = \lambda f$ (λ is wavelength, $f = 1/T$ is wave frequency).

3.2 Estimation algorithm

Establishing prior mapping relationship is a feasible way for online inlet flow velocity estimation. The remaining pressure average values are obtained to estimate flow speed according to a priori mapping: g:$C_p \rightarrow \tilde{U}$ through sensor information filtering, fluctuations and noise removal. It is assumed that there are several pressure sensors on fish surface and the associated fish wave parameters are already known. Mapping m:$p \rightarrow C_p$ is the designed sensor information filter. Mapping g:$C_p \rightarrow \tilde{U}$ is offline identified by prior data. The estimation algorithm is described as follows:

(1) Input: $p \leftarrow$ Virtual pressure sensing data

$\phi_0(f, \alpha_{\max}, \lambda) \leftarrow$Current wave motion parameters

(2) Output: $\tilde{U} \leftarrow$ Estimated flow inlet velocity

(3) Begin:

For time $t < T_s$, which is total simulation time

① $p\{\tilde{p}(x_i|t), \breve{p}(x_i|t)\} \leftarrow$ Real-time pressure sensing information with signal pre-processing;

② $p\{\tilde{p}(x_i|\tau), \breve{p}(x_i|\tau), \tau \in [0, t]\} \leftarrow$ Accumulation history sensor information;

③ $C_p \leftarrow$ Pressure coefficient generated by mapping m: $p \rightarrow C_p$;

④ $\tilde{U} \leftarrow$ Estimated flow inlet velocity, by mapping g:$C_p \rightarrow \tilde{U}$, which matches

$$\tilde{U} = \beta_0 + \beta_1 C_p + \beta_2 C_p^2 + ... + \beta_n C_p^n + \varepsilon$$

$$\varepsilon \sim N(0, \sigma^2)$$

⑤ $t \leftarrow t + \Delta t$;

End

End

If mapping h:$U \rightarrow \phi(f, \alpha_{\max}, \lambda)$ would be provided by empirical data, which means that fish can maintain force balance in flow of inlet velocity U under wave parameters. Note that $\phi(f, \alpha_{\max}, \lambda)$ is a reference value for the controller according to $\tilde{U}$, which is useful for online underwater control. The controller updates current motion parameters according to pressure sensing information, in order to achieve the balance between thrust and drag.

4 Results of flow information filtering

4.1 Scenario and set-up

About 85% of fish species use Body and/or Caudal Fin (BCF) mode, which are most aquatic creatures of high speed, high efficiency and high mobility. Fish of BCF mode generates thrust through wave travelling from the body head to tail. Body wave propagates with the wave velocity exceeding its locomotion speed in the direction opposite to cruising movement. The Reynolds number ranges between 10^3 and 10^8 in fish-like motion. As Reynolds number is the ratio of inertia force and viscous force, a large Reynolds number implies that the effect of inertia force is significant.

The parameterized kinematics law of BCF is described as

$$y(x, t) = a(x)\sin(kx - \omega t), \quad (2)$$

where $y(x, t)$ is the offset of body at body point x and time t, k is the wave number on fish body, *i.e.*, $k = 2\pi L/\lambda$, L is body length. Note that $\omega = 2\pi/T$. Also, $a(x)$ is the largest amplitude at x, which reflects the situation of fish body involved in wave motion.

Fish of BCF mode are mechanically composed of stiff anterior body and flexible rear body. Particularly, $a(x) = \alpha_{\max} e^{(1-x/L)}$ is set for anguilliform mode that the whole fish body is involved in movement. The body wave presents a flexible propulsion form.

Flexible swimming of undulation and oscillation contribute to the excellent swimming performance, such as Kármán gaiting in Kármán vortex street[3]. Either undulation of tail fin or head motion results in the disturbance of nearby flow field. Specially, the whole body

of eel is involved in wave motion, thus the corresponding disturbance and hydrodynamics are obvious. Research on the three-dimensional waving plate theory shows that as the wavelength is close to the body length, three dimensional effects almost disappear, of which hydrodynamic performance is equal to the effect of infinite two-dimensional wave plate[40]. When the wavelength is about equal to the length of fish body, the means of the lateral force and yaw moment during integral wave cycle are nearly zero. It causes smooth moving and no significant additional energy loss. It reveals why anguilliform mode is able to maintain high propulsion performance. Thus, without the loss of generality, a two-dimensional CFD model is applied in our numerical simulation. Again, the wavelength is set as $\lambda = L$. Commercial CFD software FLUENT is used to solve the fluid dynamic equations in this paper. The details of the utilized CFD model can be found in our previous works[41–43]. The numerical model has been validated for flows with moving boundaries and has also been applied successfully to simulate fish-like swimming. The computational and experimental comparison has demonstrated their consistency on the dynamic behaviors, in terms of cruising, hovering, and yawing[41].

Sensor information is a location and time correlated physical quality. The x coordinates of sensors are $\{x_i | x_i = i \cdot L/\mathrm{n},\ 0 \le i \le \mathrm{n}\}$. Sensor at head-end point is named as S_H ($i = 0$), and sensor S_T locates at tail-end point ($i = \mathrm{n}$). Two pressure sensors are set symmetrically on both sides of body at position x at time t, which are called pair sensors. Pair sensors are coded from sensor 1 to sensor (n−1), defined as S_i, $1 \le i \le \mathrm{n}-1$. $S_{i\mathrm{L}}$ locates on body's left side, and $S_{i\mathrm{R}}$ is on right side. Pressures on pair sensors are written by $\hat{p}(x_i|t)$ and $\check{p}(x_i|t)$, abbreviated as $\hat{p}_i$ and $\check{p}_i$. As for the head and tail end, $\hat{p}_0 = \check{p}_0 \triangleq p_0$, $\hat{p}_\mathrm{n} = \check{p}_\mathrm{n} \triangleq p_\mathrm{n}$.

4.2 Near-body pressure in still flow field

The pressure considered in the present work is a static pressure relative to reference pressure (*i.e*. atmospheric pressure). The pressure has a similar wave transmission process with fish wave motion. The high and low pressure zones transmit from front to back along body surface as the propulsion waveform travels. On the two sides of body surface with same x coordinates, one side drives outgoing fluid that leads to high pressure zone, and another leads to low pressure area. Fig. 5 shows the spatial-and-time distribution of near-body pressure in still water caused by fish wave motion. Periodical trends are observed in both spatial and temporal dimension. Pressures on two sides of fish body are symmetrical (Fig. 5b). Particularly, C_p on body single sensor shows the same frequency as wave motion and C_p on sensors S_H and S_T represents twice the frequency as wave motion caused by motion symmetry (Fig. 5c). The pressure is negative on the point with the widest amplitude while swimming. This is agreed with that obtained by biological experiment[44], where the pressure distribution on the fish body surface is experimentally measured. The negative pressure at the point of maximum diameter or girth can be explained from the Bernoulli principle, *i.e*. when water accelerates, the lateral pressure surrounding the fish decreases.

It is assumed that the direction of the pressure is normal to the body surface. In the cyclical fluctuations, due to the periodical body deformation in lateral direction, cyclic characteristics will be reflected in the lateral component of surface pressure. The mean of lateral force in integral cycles is nearly zero. We assume that the cyclic average of lateral pressure component on surface sampling point is approximately zero. Therefore the cyclic average pressure mainly describes numerical characteristics in forward direction. Another way to counteract pressure component on the lateral direction is to sum up the sensed pressure data of the pair-sensor mode, since the symmetric pair sensors share the same component in the vertical directions. Furthermore, the coefficients of C_p vary at the frequency twice that of the undulating locomotion, as shown in Fig. 6. The same phenomenon was in accordance with the thrust of fish-like undulating locomotion[42].

4.3 Near-body pressure effects of inlet velocity

The present work studies the hydrodynamic performance of fish-like swimming in flow field with different flow velocities. The set of flow velocities used in the simulation is $\{0, 0.2, 0.5, 0.8, 1.0\}$ $\mathrm{m \cdot s^{-1}}$. The wave motion parameters are frequency $f = 1$, and the maximum amplitude $\alpha_{\max} = 0.1\ L$. CFD numerical results are analyzed after several motion cycles, when the change of hydrodynamic features becomes stable.

The pressure signals from single sensor, symmetrical pair sensors and multiple pair sensors are

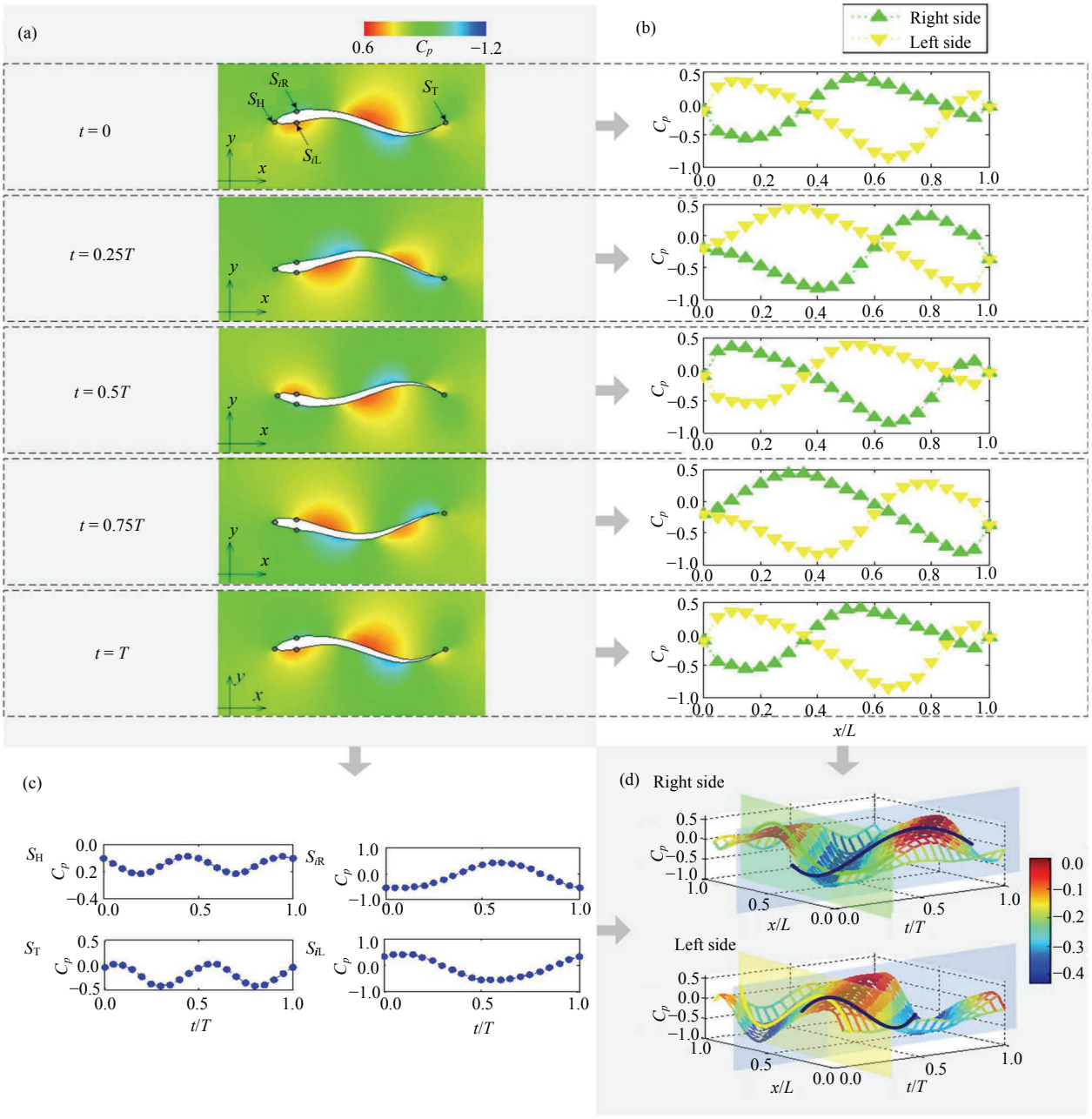

Fig. 5 The spatial-and-time distribution fish near-body pressure within still water: (a) Contour of pressure field; (b) the spatial distribution of pressure at different time; (c) the time variation of pressure from different sensors at specified points; (d) 3D view of the spatial-and-time distribution of near-body pressure.

further processed. Pressure coefficients are obtained after information filtering with the temporal and spatial operators:

(1) Single sensor coefficient

$M1$ = Average $\{p_i\}$

(2) Pair sensors coefficient

$M2$ = Average {Sum $\{\hat{p}_i, \breve{p}_i\}$}

(3) Multiple pair sensors coefficient

$M3$ = Average {Sum {Differ{shift$\{\hat{p}_i, \Delta t\}, \hat{p}_{i+1}\}$, Differ{shift$\{\breve{p}_i, \Delta t\}, \breve{p}_{i+1}\}$ }}}

The move motion phase difference of two adjacent sample points spaced by Δx is

$$\Delta\varphi = \frac{2\pi}{\lambda}\Delta x$$

The shift time is $\Delta t = \Delta x/(\lambda f)$, as calculated from $2\pi f\Delta t = 2\pi\Delta x/\lambda$.

Let us now define C_p as

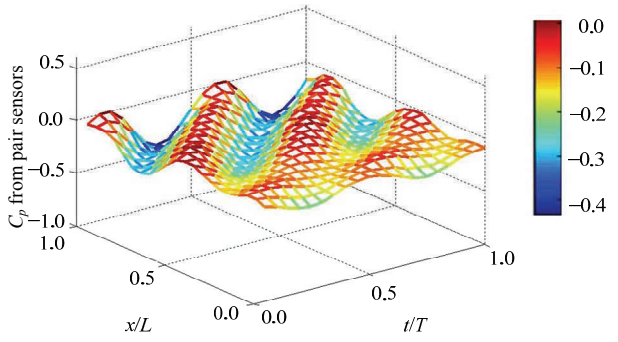

Fig. 6 Characteristics of C_p achieved from the sensed pressure data of the pair-sensor mode.

$$C_p = \frac{M}{0.5\rho U^{*2}}$$

The periodical pressure averages at different positions of single sample point showing discrepant trends, as shown in Fig. 7. It presents the trends of pressure coefficients C_p along with inlet velocity in head-on uniform flow. The inlet velocity influences obviously on near-body pressure. Pressure coefficient C_p at specific point shows a monotonous relationship with flow velocity. The experiment on real fish has demonstrated that the lateral-line is flow-sensitive to varying degrees, and the response magnitude increasing with flow rate[4]. The head end (S_H) pressure is the most sensitive to the changes of flow velocity. In addition, S_H locates at the highest pressure point (stagnation point) where the flow velocity approaches nearly zero. The trend is agreed with Bernoulli law. The pressures on the prior and rear of fish body are both related to flow velocity, but the trends of periodical pressure average are different. Sensors in prior body parts are preferred for estimation, which are more sensitive to inlet flow. Because of the symmetrical characteristic of wave motion, C_p from S_{2R} and S_{2L} are almost the same in average, but the standard deviation of C_p shows that pair sensors information is helpful to improve sensing accuracy with less data fluctuation. Fig. 8 displays the comparison of single sensor (S_{2R}), pair sensors (S_2) and multiple pair sensors (S_2 and S_3). The pressure coefficients C_p from single/multiple pair sensors are different in functional relationship with inlet velocity (Fig. 8a), whereas the amplitude of data fluctuation is similar (Fig. 8b). As sensing noise is unavoidable in physical application, any multi-sensor fusion is therefore preferred to improve the capacity of resisting disturbance.

5 Parametric study and the estimation of inlet velocity

It has been shown that the wave motion frequency and amplitude has important influence on the thrust in cruise mode of fish swimming. We will now discuss the effects of wave parameters on pressure. Given the wave parameters, a mapping from pressure coefficients to inlet velocity can be established. The inlet velocity can then be estimated according to the mapping based on the sensor information during fish-like swimming.

5.1 Near-body pressure effects of wave parameters

The pressure coefficients present similar trends in spite of some diversity along with inlet flow velocity with different parameters (Fig. 9). It is not easy to move off the effects of wave motion parameters on the pressure. However, the wave motion is an active deformation, and the wave motion parameters are known in advance. It is therefore possible to establish the relationship between inlet velocity and surface pressure with known information.

5.2 Estimation on time-varying flow inlets using head sensors

Pressure on the head end of fish body is sensitive to the inlet velocity, which can be used for estimation here. First of all, we generate the mapping of g:$C_p \rightarrow \tilde{U}$ with the results obtained above. The inlet flow velocity changes along with time in the simulation. Real-time C_p is gained from pressure sensors; then according to mapping g, the real-time $\tilde{U}$ is obtained. Flow velocity estimation algorithm includes two phases: the first is an off-line model identification, and the second is the on-line estimation. An algorithm is proposed for the flow velocity estimation. The wave frequency and amplitude are set as 1 Hz and 0.1 L, respectively in the following cases.

(1) Off-line model identification

The pressure coefficients in flow field with different inlet velocities are obtained in advance. The set of flow velocity is {0, 0.2, 0.5, 0.8, 1.0} m·s^{-1}. The model is defined in the form of polynomial, identified to be mapping g:$C_p \rightarrow \tilde{U}$ using the least squares fitting method.

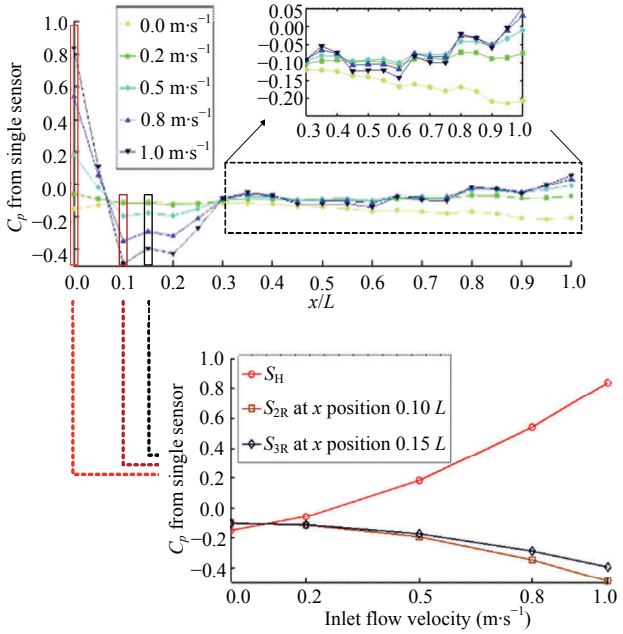

Fig. 7 Temporal change of C_p from single sensor and the trends along with inlet velocity.

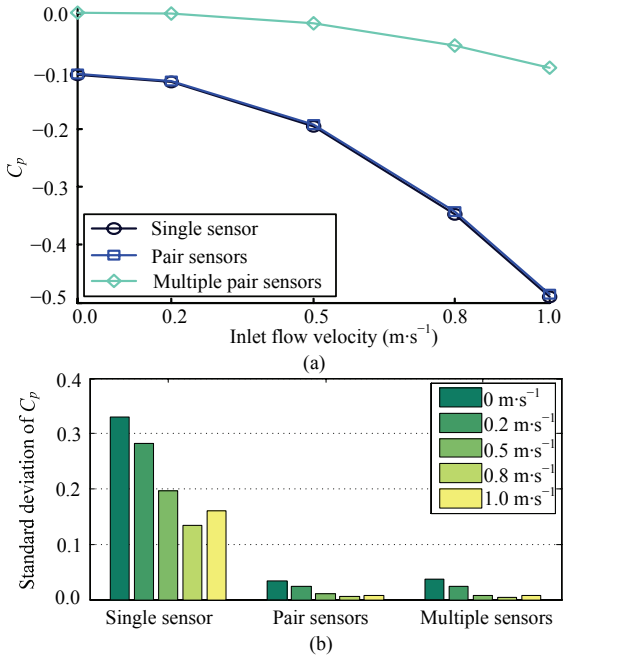

Fig. 8 Comparison of single sensor (S_{2R}), pair sensors (S_2) and multiple pair sensors (S_2 and S_3).

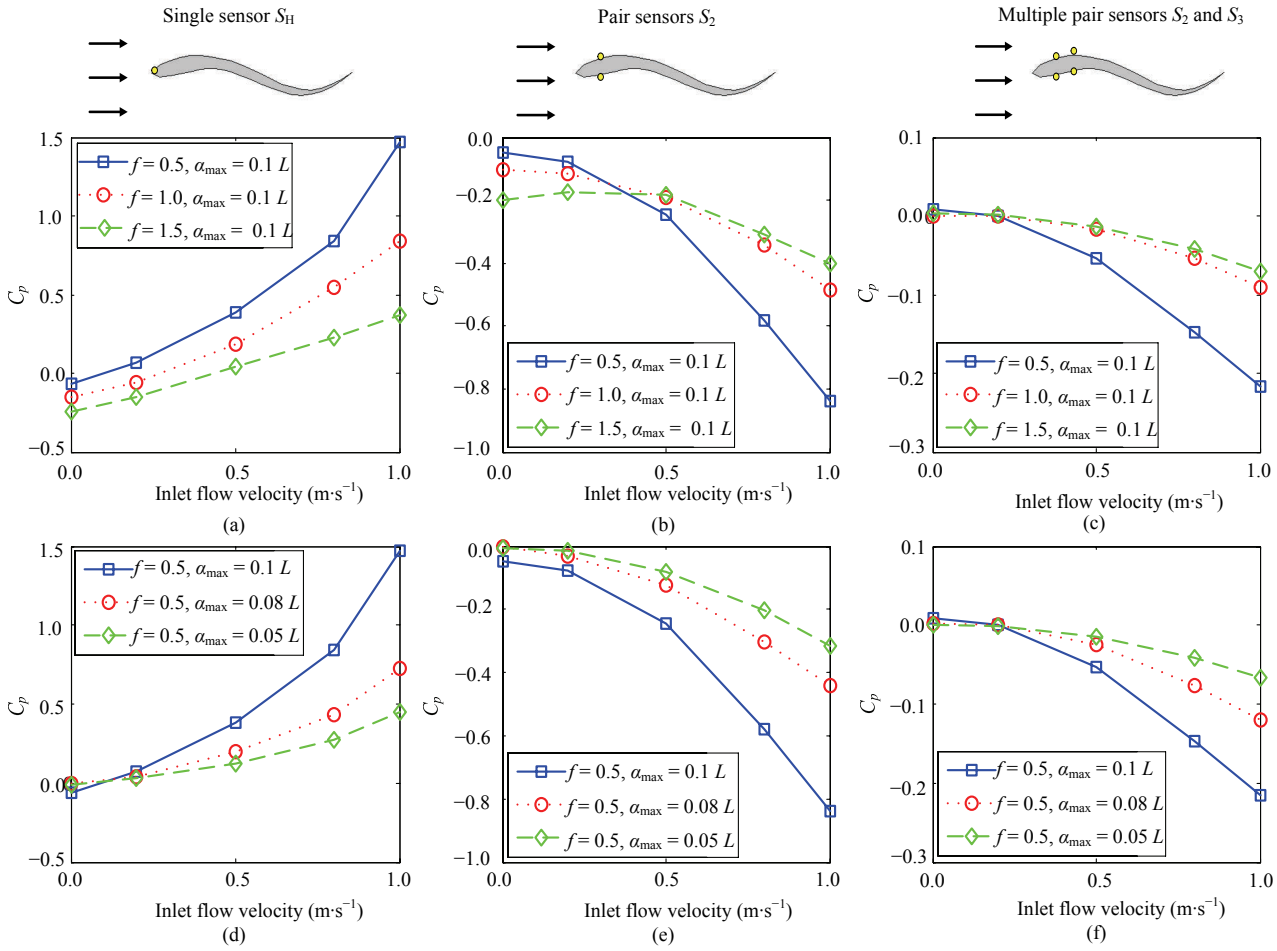

Fig. 9 Trends along with inlet velocity in different wave motion parameters.

(2) On-line estimation

As the inlet velocity changes along with time, the pressure coefficients at t are gained using near-body pressure in $[t-T, t]$ from sensors according to the filtering algorithm. The flow velocity is estimated according to mapping $g{:}C_p \rightarrow \tilde{U}$. The estimation result with pair sensors S_2 is shown in Fig. 10. The actual velocity will be taken as the initial velocity of uniform flow in the simulation set. An estimated velocity is then obtained by the proposed estimation algorithm.

Similarly, the pressure coefficients using information from sensor S_{H} are applied for estimation. Fig. 11 shows the estimation performance. The estimation error is more obvious after the moment t_S of flow velocity switching, such as $\{3, 6, 9, 12\}T$ of the case set shown in Fig. 10 and Fig. 11(a), *i.e.* the flow velocity changes every 3 cycles. The flow is going through a non-uniform phase during $[t_S, t_S+T]$. The current coefficient C_p is calculated based on pressure data of one wave cycle. When the pressure data reflects the flow effects of different velocities, as a result the estimation error increases. Fig. 11b shows another case, in which the flow velocity changes every $2T$. The estimation error is generally acceptable in our simulation cases.

The velocity estimation in a uniform inlet flow is mainly influenced by the fitting accuracy of mapping $g{:}C_p \rightarrow \tilde{U}$ and the on-line pressure sensing error. Sufficient data by fine sampling precision of flow velocities is useful for off-line model identification. Multiple pair sensors can also be used, which will then improve the anti-noise capability. The developed algorithm is suitable for the cases of staged changes of flow velocity. After the flow state has been acquired, wave motion parameters can be changed accordingly to achieve control objective. The flow sensing and filtering provide feed-forward information, and the error from sensor and the algorithm can be reduced by the feedback controller.

6 Concluding remarks

The study presented in this paper concentrated on a spatially distributed pressure sensing system that is advantageous for bio-inspired fish-like swimming. Collection and usage of temporal data from multiple sensors were fused to reduce the flow estimation uncertainty. The results of computational fluid dynamics method revealed that near-body pressure has similar characteristics

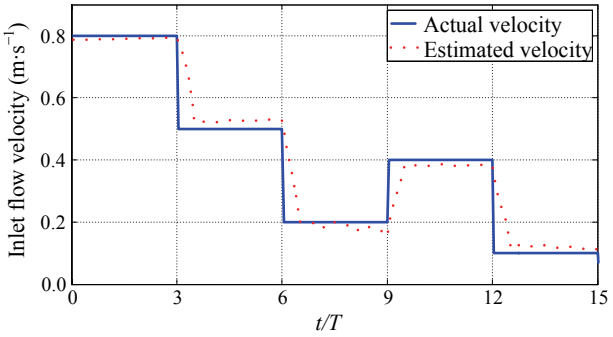

Fig. 10 Estimation result with pair sensors S_2.

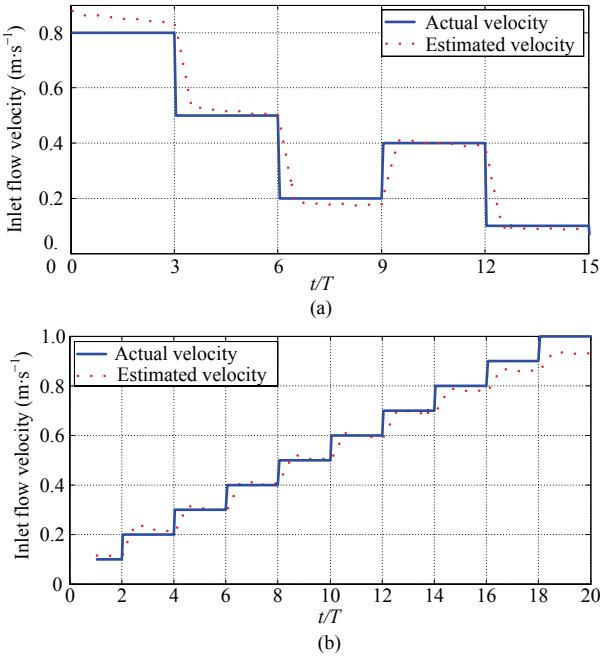

Fig. 11 Estimation result with sensor S_{H} in different cases: (a) The flow velocity changes at every three cycles and the velocity either increases or decreases at the switching moment; (b) the flow velocity changes at every two cycles and the flow velocity changes incrementally.

with wave motion, such as periodicity and symmetry. Wave motion parameters and inlet flow velocity will both affect the perception of sensors, which has an important influence on flow prediction and controller design. The cyclic average value of pressure is preferred to predict inlet flow velocity in a uniform flow.

In the near future, flow estimation using distributed pressure sensing should be an inspiring and practical topic in the field of bio-inspired underwater locomotion. It does not only contribute to understanding inherence of lateral lines, but also draws inspirations for improving the adaptability of robotic fish prototypes within complicated environments. Eventually, more compact flow

sensors and more accurate estimation algorithms are both in great need. They are to be developed to eliminate the influence of wave motion and disturbance, and meanwhile to unveil the essence of fish-like swimming flows. Furthermore, flow sensing and prediction of instantaneous unsteady flows or obstacle-induced vortex streets will be great challenges in this field.

Acknowledgment

This work was supported in part by the National Science Foundation of China under Grant nos. 61005077, 51105365 and 61273347, in part by Research Fund for the Doctoral Programme of Higher Education of China under Grant no. 20124307110002, and in part by the Foundation for the Author of Excellent Doctoral Dissertation of Hunan Province under Grant no. YB2011B0001.

The authors would like to thank Daibing Zhang for his sincere guidance and constructive comments. The corresponding author (Tianjiang hu) would like to thank Dr. Xue-feng Yuan of University of Manchester, UK for the collaboration during Dr. Hu's academic visit from February 2013 to August 2013 in Manchester Institute of Biotechnology.

References

[1] Fish F E, Lauder G V. Passive and active flow control by swimming fishes and mammals. *Annual Review of Fluid Mechanics*, 2006, **38**, 193–224.

[2] Wen L, Waver J, Lauder G V. Biomimetic shark skin: Design, fabrication and hydrodynamic testing. *The Journal of Experimental Biology*, 2014, **217**, 1637–1638.

[3] Liao J C. A review of fish swimming mechanics and behaviour in altered flows. *Philosophical Transactions of the Royal Society B*, 2007, **362**, 1973–1993.

[4] Voigt R, Carton A G, Montgomery J C. Responses of anterior lateral line afferent neurones to water flow. *The Journal of Experimental Biology*, 2000, **203**, 2495–2502.

[5] Przybilla A, Kunze S, Rudert A, Bleckmann H, Brücker C. Entraining in trout: A behavioural and hydrodynamic analysis. *The Journal of Experimental Biology*, 2010, **213**, 2976–886.

[6] Coombs S, Bleckmann H, Fay R R. *The Lateral Line System*, Springer, New York, 2014.

[7] Webb J F. Gross morphology and evolution of the mechanosensory lateral line system in teleost fishes. *Brain, Behavior and Evolution*, 1989, **33**, 34–53.

[8] Liu J D, Hu H. Biologically inspired behaviour design for autonomous robotic fish. *International Journal of Automation and Computing*, 2006, **3**, 336–347.

[9] Triantafyllou M S, Triantafyllou G S. An efficient swimming machine. *Scientific American*, 1995, **272**, 62–70.

[10] Wen L, Wang T M, Wu G H. Hydrodynamic investigation of a self-propulsive robotic fish based on a force-feedback control method. *Bioinspiration & Biomimetics*, 2012, **7**, 036012.

[11] Kato N. Median and paired fin controllers for biomimetic marine vehicles. *Applied Mechanics Reviews*, 2005, **58**, 238–252.

[12] Hu T J, Shen L C , Lin L X. Biological inspirations, kinematics modeling, mechanism design and experiments on an undulating robotic fin inspired by *Gymnarchus Niloticus*. *Mechanism and Machine Theory*, 2009, **44**, 633–645.

[13] Zhou C L, Low K H, Chong C W. An analytical approach for better swimming efficiency of slender fish robots based on Lighthill's model. *IEEE International Conference on Robotics and Biomimetics*, Guilin, China, 2009, 1651–1656.

[14] Low K H, Chong C W. Parametric study of the swimming performance of a fish robot propelled by a flexible caudal fin. *Bioinspiration & Biomimetics*, 2010, **5**, 046002.

[15] Wen L, Wang T M, Wu G H, Liang J H. Hydrodynamic performance of an undulatory robot: Functional roles of the body and caudal fin locomotion. *International Journal of Advanced Robotic System*, 2013, **9**, 1–10.

[16] Dusek J, Kottapalli A G P, Woo M E, Asadnia M, Miao J, Lang J H, Triantafyllou M S. Development and testing of bio-inspired microelectromechanical pressure sensor arrays for increased situational awareness for marine vehicles. *Smart Materials and Structures*, 2013, **22**, 014002.

[17] Yang Y C, Chen J, Engel J, Pandya S, Chen N, Tucker C, Coombs S, Jones D L, Liu C. Distant touch hydrodynamic imaging with an artificial lateral line. *Proceedings of the National Academy of Sciences of the United States of America* (*PNAS*), 2006, **103**, 18891–18895.

[18] Abdulsadda A T, Tan X B. Nonlinear estimation-based dipole source localization for artificial lateral line systems. *Bioinspiration & Biomimetics*, 2012, **8**, 026005.

[19] Fernandez V I, Maertens A, Yaul F M, Dahl J, Lang J H, Triantafyllou M S. Lateral-line-inspired sensor arrays for navigation and object identification. *Marine Technology Society Journal*, 2011, **45**, 130–146.

[20] Bouffanais R, Weymouth G D, Yue D K P. Hydrodynamic object recognition using pressure sensing. *Proceedings of the Royal Society A*, 2010, **467**, 19–38.

[21] Venturelli R, Akanyeti O, Visentin F, Ježov J, Chambers L

D, Toming G, Brown J, Kruusmaa M, Megill W M, Fiorini P. Hydrodynamic pressure sensing with an artificial lateral line in steady and unsteady flows. *Bioinspiration & Biomimetics*, 2012, **7**, 036004.

[22] Chambers L D, Akanyeti O, Venturelli R, Ježov J, Brown J, Kruusmaa M, Fiorini P, Megill W M. A fish perspective: detecting flow features while moving using an artificial lateral line in steady and unsteady flow. *Journal of the Royal Society Interface*, 2014, **11**, 20140467.

[23] DeVries L, Paley D A. Observability-based optimization for flow sensing and control of an underwater vehicle in a uniform flowfield. *American Control Conference*, Washington D. C., USA, 2013, 1386–1391.

[24] Lagor F D, DeVries L D, Waychoff K M, Paley D A. Bio-inspired flow sensing and control for autonomous underwater navigation using distributed pressure measurements. *Proceedings of* 18*th International Symposium on Unmanned Untethered Submersible Technology*, Portsmouth, New Hampshire, 2013.

[25] Salumäe T, Kruusmaa M. Flow-relative control of an underwater robot. *Proceedings of the Royal Society*, 2013, **469**, 20120671.

[26] Ježov J, Akanyeti O, Chambers L D, Kruusmaa M. Sensing oscillations in unsteady flow for better robotic swimming efficiency. *Proceedings of IEEE International Conference on Systems*, *Man and Cybernetics*, Seoul, Korea, 2012, 91–96.

[27] Ayali A, Gelman S, Tytell E D, Cohen A H. Lateral-line activity during undulatory body motions suggests a feedback link in closed-loop control of sea lamprey swimming. *Canadian Journal of Zoology*, 2009, **87**, 671–683.

[28] Akanyeti O, Chambers L D, Ježov J, Brown J, Kruusmaa M, Megill W M, Fiorini P. Self-motion effects on hydrodynamic pressure sensing: Part I. forward-backward motion. *Bioinspiration & Biomimetics*, 2013, **8**, 026001.

[29] Liu H, Wassersug R J, Kawachi E. A computational fluid dynamics study of tadpole swimming. *The Journal of Experimental Biology*, 1996, **199**, 1245–1260.

[30] Carling J, Williams T L, Bowtell G. Self-propelled anguilliform swimming: Simultaneous solution of the two-dimensional navier-stokes equations and newton's laws of motion. *The Journal of Experimental Biology*, 1998, **201**, 3143–3166.

[31] Wolfgang M J, Anderson J M, Grosenbaugh M A, Yue D K, Triantafyllou M S. Near-body flow dynamics in swimming fish. *The Journal of Experimental Biology*, 1999, **202**, 2303–2327.

[32] Borazjani I, Sotiropoulos F. Numerical investigation of the hydrodynamics of carangiform swimming in the transitional and inertial flow regimes. *The Journal of Experimental Biology*, 2008, **211**, 1541–1558.

[33] Shirgaonkar A A, MacIver M A, Patankar N A. A new mathematical formulation and fast algorithm for fully resolved simulation of self-propulsion. *Journal of Computational Physics*, 2009, **228**, 2366–2390.

[34] Bergmann M, Iollo A. Modeling and simulation of fish-like swimming. *Journal of Computational Physics*, 2011, **230**, 329–348.

[35] Wen L, Wang T M, Wu G H, Liang J H. Quantitative thrust efficiency of a self-propulsive robotic fish: Experimental method and hydrodynamic investigation. *IEEE/ASME Transactions on Mechatronics*, 2013, **18**, 1027–1038.

[36] Rapo M A, Jiang H S, Grosenbaugh M A, Coombs S. Using computational fluid dynamics to calculate the stimulus to the lateral line of a fish in still water. *The Journal of Experimental Biology*, 2009, **212**, 1494–1505.

[37] Windsor S P, Norris S E, Cameron S M, Mallinson G D, Montgomery J C. The flow fields involved in hydrodynamic imaging by blind Mexican cave fish (Astyanax fasciatus). Part I: Open water and heading towards a wall. *The Journal of Experimental Biology*, 2010, **213**, 3819–3831.

[38] Windsor S P, Norris S E, Cameron S M, Mallinson G D, Montgomery J C. The flow fields involved in hydrodynamic imaging by blind Mexican cave fish (Astyanax fasciatus). Part II: Gliding parallel to a wall. *The Journal of Experimental Biology*, 2010, **213**, 3832–3842.

[39] Barbier C, Humphrey J A. Drag force acting on a neuromast in the fish lateral line trunk canal. I. Numerical modelling of external-internal flow coupling. *Journal of the Royal Society Interface*, 2009, **6**, 627–640.

[40] Cheng J Y, Zhuang L X, Tong B G. Analysis of swimming three-dimensional waving plates. *Journal of Fluid Mechanics*, 1991, **232**, 341–355.

[41] Zhou H, Hu T J, Xie H B, Zhang D B, Shen L C. Computational and Experimental study on dynamic behavior of underwater robots propelled by bionic undulating fins. *Science China Technological Sciences*, 2010, **53**, 2966–2971.

[42] Hu T J, Low K H, Shen L C, Xu X. Effective phase tracking for bioinspired undulations of robotic fish models: A learning control approach. *IEEE/ASME Transactions on Mechatronics*, 2014, **19**, 191–200.

[43] Zhou H, Hu T J, Wang G M, Zhang D B, Lv Y X. Simulation platform for fishlike swimming. *Applied Mechanics and Materials*, 2014, **461**, 451–458.

[44] Dubois A, Cavagna G A, Fox R S. Pressure distribution on the body surface of swimming fish. *The Journal of Experimental Biology*, 1974, **60**, 581–591.